



HAL
open science

Printing polarization and phase at the optical diffraction limit: near and far-field optical encryption

Qinghua Song, Samira Khadir, Stéphane Vézian, Benjamin Damilano, Philippe de Mierry, Sébastien Chenot, Virginie Brandli, Romain Laberdesque, Benoit Wattellier, Patrice Genevet

► To cite this version:

Qinghua Song, Samira Khadir, Stéphane Vézian, Benjamin Damilano, Philippe de Mierry, et al.. Printing polarization and phase at the optical diffraction limit: near and far-field optical encryption. *Nanophotonics*, 2020, 10 (1), pp.697-704. 10.1515/nanoph-2020-0352 . hal-03582590

HAL Id: hal-03582590

<https://hal.science/hal-03582590>

Submitted on 21 Feb 2022

HAL is a multi-disciplinary open access archive for the deposit and dissemination of scientific research documents, whether they are published or not. The documents may come from teaching and research institutions in France or abroad, or from public or private research centers.

L'archive ouverte pluridisciplinaire **HAL**, est destinée au dépôt et à la diffusion de documents scientifiques de niveau recherche, publiés ou non, émanant des établissements d'enseignement et de recherche français ou étrangers, des laboratoires publics ou privés.

Printing polarization and phase at the optical diffraction limit: near and far-field optical encryption

Qinghua Song¹, Samira Khadir¹, Stéphane Vézian¹, Benjamin Damilano¹, Philippe de Mierry¹, Sébastien Chenot¹, Virginie Brandli¹, Romain Laberdesque², Benoit Wattellier², and Patrice Genevet¹

¹ Université Cote d'Azur, CNRS, CRHEA, Rue Bernard Gregory, Sophia Antipolis 06560 Valbonne, France

² Phasics Company, Bâtiment Explorer, Espace Technologique, Route de l'Orme des Merisiers, 91190 St Aubin, France

† Corresponding Author: Patrice.Genevet@crhea.cnrs.fr

Abstract: Securing optical information to avoid counterfeiting and manipulation by unauthorized persons and agencies requires innovation and enhancement of security beyond basic intensity encryption. In this paper, we present a new method for polarization-dependent optical encryption that relies on extremely high resolution near-field phase encoding at metasurfaces, down to the diffraction limit. Unlike previous intensity/color printing methods, which are detectable by human eye, analogue phase decoding requires specific decryption setup to achieve higher security level. In this work, quadriwave lateral shearing interferometry is used as a phase decryption method, decrypting binary quick response (QR) phase codes, and thus forming phase contrast images, with phase values as low as 15°. Combining near field phase imaging and far field holographic image under orthogonal polarization illumination, we enhanced the security level for potential applications in the area of biometrics recognition, secure ID cards, secure optical data storage, steganography and communications.

Keywords: Information security, nanoantenna, optical encryption, dielectric metasurface, meta-hologram.

1 Introduction

Information security is an important concern in the daily life from civil to military applications [1,2]. Optical encryption for the information security has gained enormous attention due to its ability to provide many degrees of freedom to encode the information relying on various optical channels such as frequency, amplitude, phase and polarization [3,4]. These efforts led to various encryption methods, including Lippmann plate [5], spatial correlators [6], and holograms [7]. Recently, an ultra-thin artificial material with subwavelength structures called metasurface [8-10] has been developed to control the electromagnetic wave across the entire frequency range for various optical applications such as lenses [11-15], cloaking [16-17], holograms [18-21], polarizers [22-24], perfect absorbers [25-26], retroreflectors [27], etc. The compactness and versatile functionality make metasurfaces perfect candidates for the optical encryption. The basic idea is to leverage on different optical channels of the metasurface to encode different optical information. Proof of concept demonstration of metasurface spectral encoding, displaying sharp and hyper-resolved images observable under a microscope, have been demonstrated [28,29]. Metasurfaces have also been designed to perform far field holographic encoding using the concept of meta-holograms. The latter is the most common approach in the area of metasurface encryption using different light source to decrypt the holographic images. A great deal of attention has been paid on the design of light source dependent meta-hologram, such as polarization selectivity [30-33], orbital angular momentum selectivity [34,35], incoming direction of the incident light [36-38], etc. Other attempts have also been made for metasurface encryption, such as the combination of the color printing and holographic image [39,40], image post-processing based on spatial frequency [41], and tunable meta-hologram [42]. All of the proposed metasurface encryptions, either relying on the intensity of the color print or on the holographic image projection, are directly perceived by human eyes, which could limit their applicability for information security.

Here, we introduce a new class of optical encryption that combines the near and far field information. On the one hand, the near field encryption is based on phase imaging at the metasurface plane. The information is encoded in the phase of the transmitted light without any modulation of its intensity, making the information inaccessible with conventional microscope. In order to resolve the encoded information, one has to obtain the phase map information, which we measured in this article using quadriwave lateral shearing interferometry (QLSI) technique [43-46] (see more details in Methods). The phase addressing capability of metasurfaces, i.e. the spatial phase distribution of the phase elements, can be scale down to the single pixel with a pitch of 300 nm, which is beyond the Abbe's classical diffraction

limit with incident wavelength higher than 600 nm. Obviously, as to retrieve the phase information, one is using traditional optical characterization tools generally limited to the diffraction limits, it is not necessary to encode with such offensive resolution. As a proof of concept, we have considered phase pixels of about 750 nm. The proposed phase encryption could complement the class of colour printing at the optical diffraction limit [28,29] in high-density spectrally encoded optical data storage, etc. On the other hand, far field encryption relying on holographic image requires a full 2π phase range, which according to our results, appears to be not necessary for near field encoding mentioned above, allowing more flexibility for realistic applications. The combination of phase and projected intensity, respectively encoded in the near field and far field, improves the optical information security.

In the following section, we describe the theoretical design as well as the experimental fabrication and characterization methods. Two different examples of phase encryption are demonstrated in section 3. The first example shows several functional phase encoded binary quick response (QR) codes with decreasing phase encoding values ranging from 180° down to 15° phase difference, below which the experimental realization fails to deliver readable codes. In the second example, near field encryption, i.e. phase imaging at the metasurface plane, is multiplexed with far field encryption, i.e. holographic image projection, to display two different “Bat” and “Batman” images.

2 Design and fabrication

The principle of the dual-mode encryption is shown in Figure 1. The metasurface consists of a birefringent dielectric meta-molecule array with Jones matrix of $\begin{pmatrix} J_{xx} & 0 \\ 0 & J_{yy} \end{pmatrix} = \begin{pmatrix} e^{i\varphi_{xx}} & 0 \\ 0 & e^{i\varphi_{yy}} \end{pmatrix}$ (assuming full transmission of the incident wave). When a plane wave with x -polarization (\mathbf{E}_x) illuminates the metasurface as shown in Figure 1B left panel, the output near field of the metasurface is $\mathbf{E}_x e^{i\varphi_{xx}}$, which is encoded by a phase information of φ_{xx} . By locally designing different meta-structures, we can get a specific phase pattern in the near field (Figure 1B middle) and a random intensity profile in the far field (Figure 1B right). However, the y -polarized light works in the opposite way, creating a disordered near field phase image but encrypting a holographic image in the far field as shown in Figure 1C.

The design of the metasurfaces is realized using full-wave finite-difference time-domain (FDTD) simulations at the wavelength of 617 nm. The unit-cell of the metasurface consists of semiconductor-based GaN nanopillars with thickness of $h = 1 \mu\text{m}$ and period of $P = 300 \text{ nm}$ on sapphire substrate as shown in Figure 2A and 2B. GaN has the merits of 1) low loss in the entire visible range to design the metasurfaces with high efficiency, 2) high refractive index to manipulate the phase in full 2π range using relatively short nanostructures. Other low loss and high refractive index like SiN and TiO_2 could be alternative choices [47, 48]. The GaN nanopillars support waveguide-like modes for which the accumulated phase of the transmitted light is strongly dependent on the dimension L_x and L_y [13]. The simulated results of the transmitted amplitude and phase, shown in Figure 2C-2E, demonstrate that the transmitted amplitude of the metasurface is almost near-unity, while the phase is widely covering a full 2π range.

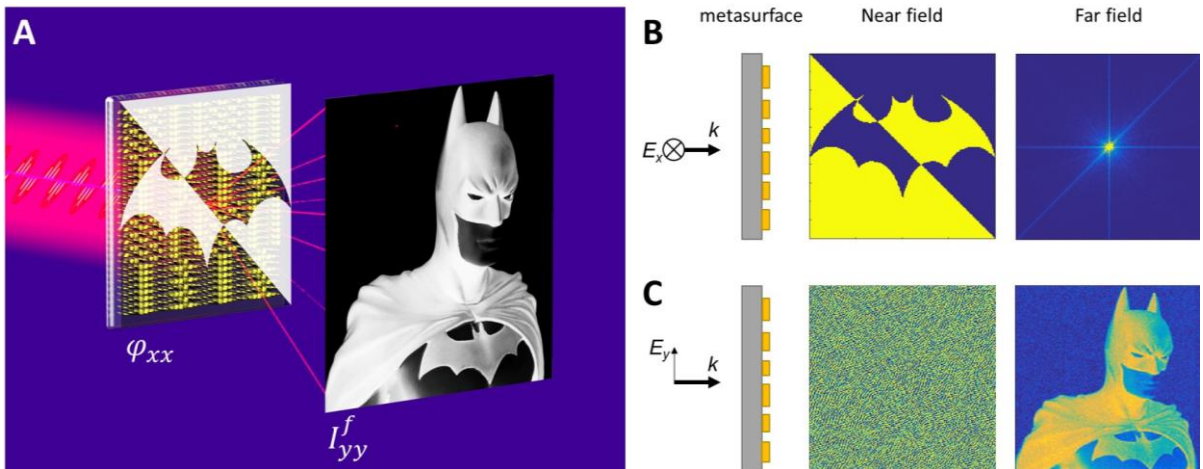


Figure 1: Design principle of dual-mode encryption combining near field phase imaging and far field holographic image projection. (A) Schematic of the dual-mode encryption, in which the near field is encrypted by a phase imaging of “Bat” and the far field is encrypted by a holographic image of “Batman”. (B) Metasurface under x -polarized incidence (left panel). A phase imaging of “Bat” is retrieved by extracting the metasurface spatial phase distribution (middle panel). A random intensity profile is displayed

in the far field (right panel). (C) Metasurface under y -polarized incidence (left panel). Complex holographic phase imaging is observed (middle panel). A holographic image of “Batman” is observed in the far field (right panel). “Bat” and “Batman” images are adapted from Wikimedia.org and Pexels.com, respectively.

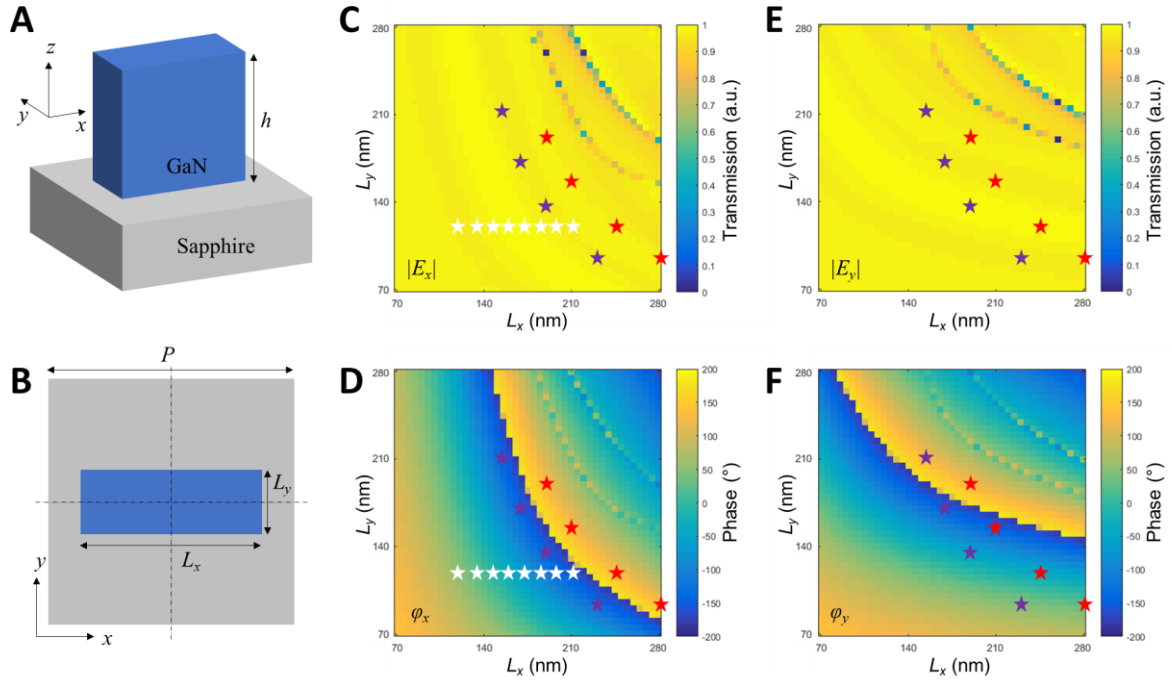


Figure 2: Simulation results of metasurface consisting of GaN nano-pillars on sapphire substrate. (A) Perspective view and (B) top view of the metasurface with one meta-molecule. (C) Simulated amplitude and (D) phase of the transmission with x -polarized incidence. (E) Simulated amplitude and (F) phase of the transmission with y -polarized incidence by changing the size of the GaN blocks. The white stars are the selected structures for the design of SC-MS. The purple and red stars are selected for the design of DC-MS.

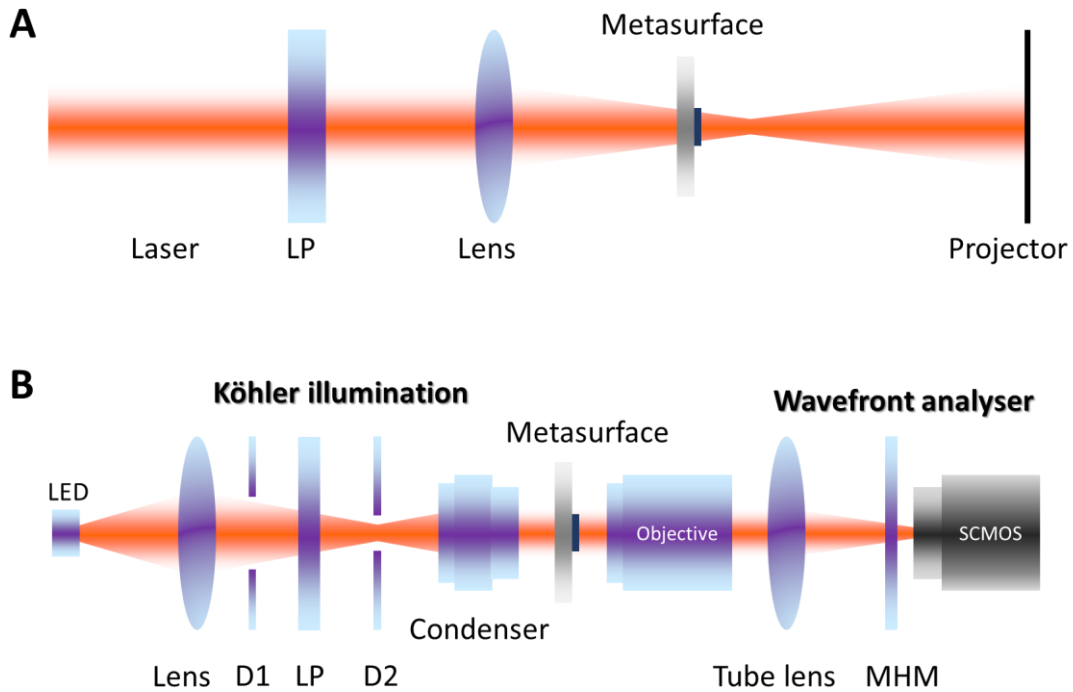


Figure 3: Measurement setup for dual-mode encryption. (A) Optical setup for far field holographic image under illumination of laser at wavelength of 617 nm. (B) Phase imaging measurement setup using QLSI. A LED with a wavelength centered at 617

nm integrated in a Köhler configuration is used as an illumination source on the metasurface with a controlled optical plane wave. The transmitted signal is then collected by the wavefront analyser. D1 and D2 are field and aperture diaphragms respectively. LP: linear polarizer. MHM: modified Hartmann mask. SCMOS: scientific complementary metal-oxide-semiconductor.

In the following, we propose two sets of encrypting metasurfaces, a) a single-channel metasurfaces (SC-MS) encryption working only for x -polarized light and b) a dual-channel metasurfaces (DC-MS) encryption that works differently for x - and y -polarized light. SC-MS keeps $L_y = 120$ nm and L_x is controlled to achieve different phase information for x -polarized light as shown by the white stars in Figure 2C and 2D. DC-MS controls both phase information of x - and y -polarized light as shown in the purple and red stars in Figure 2C-2F. By controlling the size of L_x and L_y of the DC-MS, the transmitted phase of x -polarized light φ_{xp} and φ_{xr} (subscript “ p ” indicates purple stars and “ r ” for red stars) are constant along the purple and red stars respectively with a phase difference $\varphi_{xp} - \varphi_{xr}$ of 90° for binary phase imaging in the near field. Meanwhile, the phase of the y -polarized light φ_{yp} and φ_{yr} vary in 2π range for the phase encoding of holographic image in the far field. For simplicity, the holographic phase profile has been encoded in only 4 phase levels.

3 Results and discussion

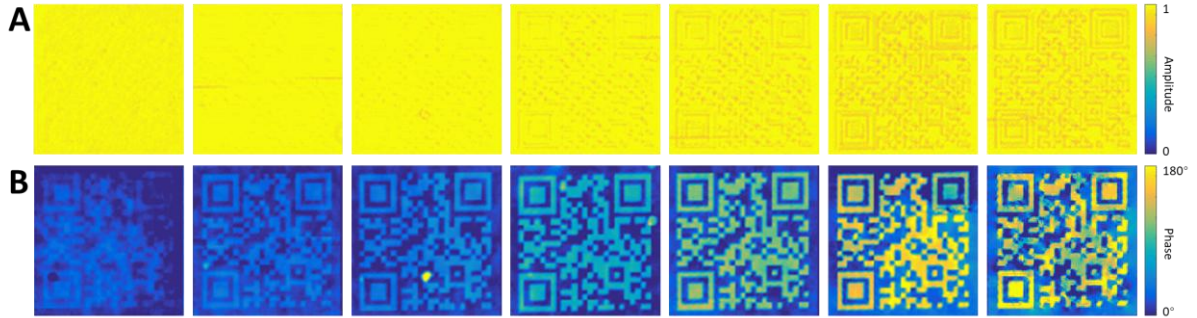


Figure 4: Experimental results of binary QR codes using SC-MS. (A) Amplitude and (B) phase images measured by QLSI. From left to right panels, the expected binary phase contrast values are 5° , 15° , 30° , 60° , 90° , 135° , and 180° (all the phase images have the same scale of 0° to 180°). The QR code is designed to link CNRS-CRHEA website (www.crhea.cnrs.fr). The phase images with binary phase contrast $\geq 15^\circ$ can be redirected to the CNRS-CRHEA website when scanned by a portable QR code scanner, and it starts to fail for extremely small phase contrast below 5° . The size of the QR code is $174 \mu\text{m} \times 174 \mu\text{m}$.

As a proof of concept, we demonstrate a binary quick response (QR) code in the SC-MS with binary encoded phase of φ_h and φ_l (subscripts of “ h ” and “ l ” indicate high- and low-level phase, respectively) for the phase imaging. The QR code consists of 29×29 pixels with binary phase of φ_h and φ_l , which redirects to the CNRS-CRHEA website when it is scanned by a portable QR code scanner. Each pixel of the QR code contains 20×20 meta-structures. Thus, the total size of the SC-MS is $174 \mu\text{m} \times 174 \mu\text{m}$. We fabricate seven samples of SC-MS with different phase contrast $\Delta\varphi = \varphi_h - \varphi_l$ ranging from 5° , 15° , 30° , 60° , 90° , 135° , and 180° . The measurement setup for the phase imaging is shown in Figure 3 (see more details of measurement setup in Methods). The measured amplitude and phase profile using QLSI are shown in Figure 4A and 4B, respectively. One can see that the QR codes are almost invisible on the amplitude images and are thus impossible to read while they are clearly visible on the phase images. When the phase contrast $\Delta\varphi \geq 15^\circ$, the measured QR code phase images can be scanned and directed to the CNRS-CRHEA website but it starts to fail when $\Delta\varphi \leq 5^\circ$. In order to estimate the actual values of $\Delta\varphi$ of the measured QR code phase images, we plot the pixel-by-pixel histograms for each image as shown on Figure 5A. The histogram is fitted with Gaussian functions with two peaks, one corresponding to the low-level phase φ_l and the other to high-level phase φ_h . The difference between the two peaks gives the phase contrast $\Delta\varphi$ while the full width at half maximum estimates the error of the extracted phase. The results for different phase contrast from 15° to 180° are shown on Figure 5A. The expected, measured phase and standard deviation of φ_h and φ_l are shown in Figure 5B.

It can be seen that when $\Delta\varphi$ is too small, $\Delta\varphi = 5^\circ$, the width of each Gaussian profile is larger than $\Delta\varphi$, which makes the two peaks indistinguishable. The discrepancy of the measured phase mainly comes from the fabrication error, since the length difference of the GaN nanopillars corresponding to the binary phase of 5° is only 2.5 nm which

is lower than our e-beam lithography precision. Increasing the designed phase contrast, i.e. such as $\Delta\varphi \geq 15^\circ$, the two peaks become distinguishable and the extracted phase contrasts agree well with the expected ones. However, when the phase contrast is close to 180° , such as $\Delta\varphi = 135^\circ$ and $\Delta\varphi = 180^\circ$, the standard deviation is increasing due to the phase wrapping issues from the phase retrieval algorithm used to extract the pixel phase value.

The near field phase imaging can be further combined with far field holographic imaging, so that a dual-mode optical encryption can be achieved. Here the phase contrast of near field phase imaging is chosen as $\Delta\varphi = 90^\circ$, according to its good performance observed in Figure 5. The experimental results of DC-MS for near field and far field encryption are shown in Figure 6A. When the metasurface is illuminated by x -polarized light, a phase image of “Bat” measured by QLSI is shown in Figure 6B, however, due to the designed phase in the near field only, the holographic image in the far field has no useful information as shown in Figure 6C. Instead, considering a y -polarized light illumination, a phase profile without useful information is shown in Figure 6D, displaying a holographic image of “Batman” in the far field as shown in Figure 6E to achieve a dual-mode optical encryption able to combine near field phase imaging and far field holographic image projection.

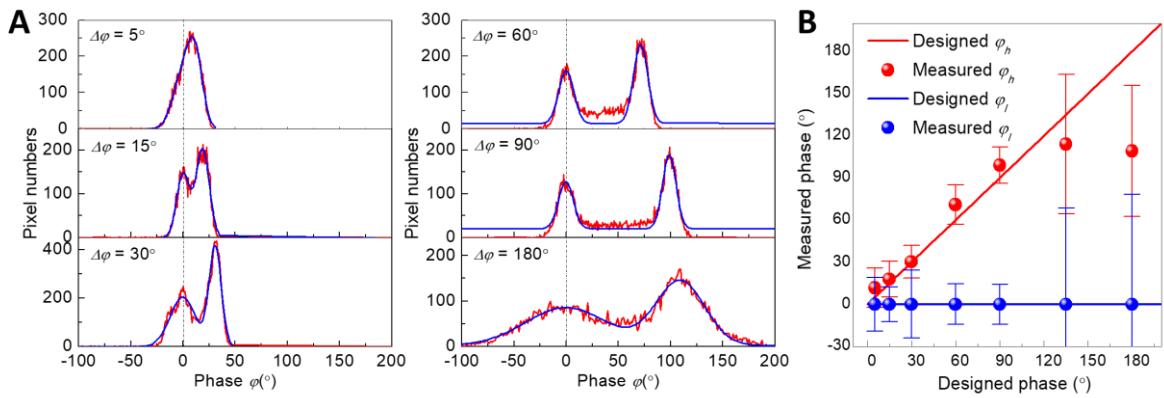


Figure 5: (A) Pixel-by-pixel histogram of the measured phase images for the different designed phase contrast of $5^\circ, 15^\circ, 30^\circ, 60^\circ, 90^\circ,$ and 180° . Red curve: measured results. Blue curve: fitting curves based on two Gaussian functions. (B) The measured phase and standard deviation of binary phase imaging.

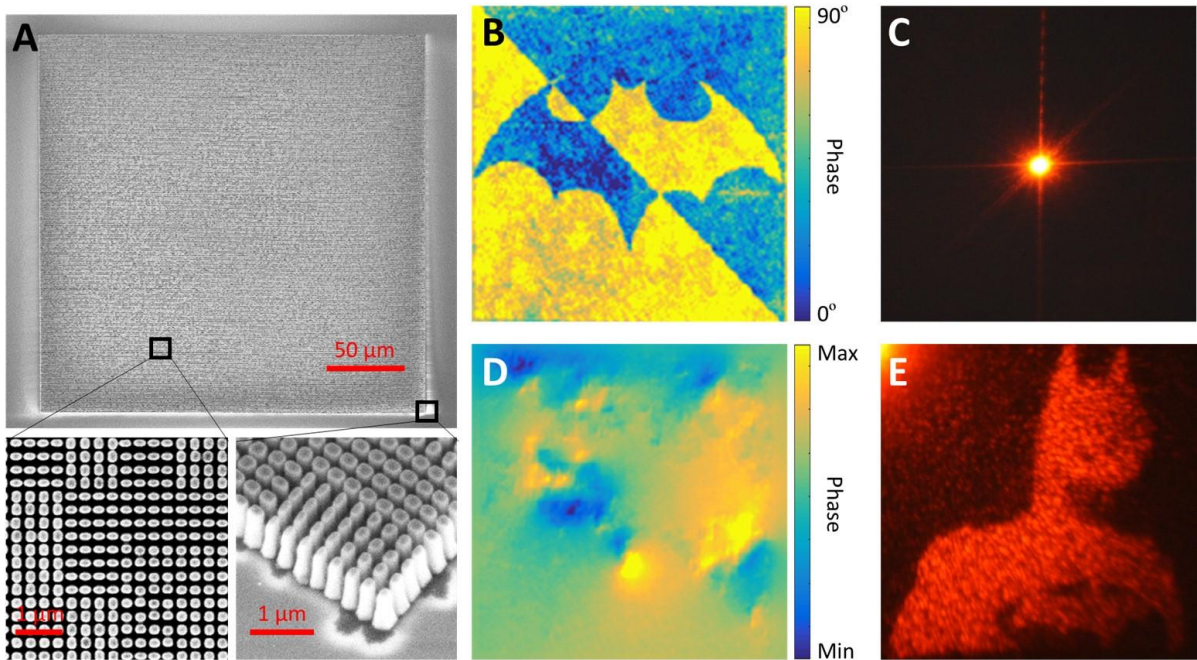


Figure 6: Experimental results of DC-MS. (A) SEM images of the fabricated metasurface. (B) Measured phase image and (C) far field with x -polarized incidence. (D) Measured phase image and (E) far field holographic image with y -polarized incidence.

4 Conclusion

In conclusion, we have demonstrated a new class of optical encryption relying on dual mode metasurfaces. Our method is able to print optical phase information at nanoscale, and which can be extracted using QLSI technique. We encoded several phase QR codes in simple binary phase images, demonstrating significant advantage with respect to conventional full phase holographic image encryption. We demonstrated that a phase difference as low as 15° is sufficient to successfully scan the QR code and redirect to the desired website page. It is interesting to point out that gradually varying the nanopillar geometry enables analogue phase addressing, offering interesting perspective for multiplexed coding capabilities. Moreover, by combining the holographic display in the orthogonal polarization, a dual-mode optical encryption is demonstrated for the near field and far field encryption, expanding promising applications in the optical information security, data encryption, optical ID tags for authentication and verification, high-density optical data storage, etc.

Acknowledgments: The authors acknowledge the support from the European Research Council (ERC) under the European Union's Horizon 2020 research and innovation programme (Grant agreements no. 639109).

5 Methods

5.1 Fabrication processes

The fabrication of the metasurface starts from growing a $1\ \mu\text{m}$ GaN thin-film on a double-side polished c-plane sapphire substrate using a molecular beam epitaxy (MBE) RIBER system. Conventional electron beam lithography (EBL) is used to pattern the GaN nanopillars. The GaN thin-film is spin-coated by a double layer of 200 nm PMMA resist (495A4) and baked on a hot-plate with temperature of 125°C . The resist is exposed to an electron beam of 20 keV (Raith ElphyPlus, Zeiss Supra 40) considering the desired pattern and then developed using IPA:MIBK (3:1) solution. A 50 nm thick Nickel film is deposited on the sample in the E-beam evaporator and a Nickel hard mask is obtained by removing the resist through lift-off process in acetone solution. The GaN nanopillars are obtained by reactive ion etching (RIE, Oxford system) with a plasma composed of $\text{Cl}_2\text{CH}_4\text{Ar}$ gases. Finally, the Nickel hard mask on the GaN nanopillars is dissolved in $\text{HCl}:\text{HNO}_3$ (1:2) solution, revealing only the GaN nanopillars pattern on the transparent sapphire substrate.

5.2 Measurement setup

The measurement setup for the far field holographic image is shown in Figure 3A. A laser with a wavelength of 617 nm is used as the light source. The latter passes through a linear polarizer (LP) followed by a lens to weakly focus on the metasurface and creates a holographic image in the far field, which is captured by a projector placed after the metasurface at a distance of 10 cm. The setup for the phase imaging is shown on Figure 3B. It utilizes a quantitative phase microscopy technique based on Quadriwave Lateral Shearing Interferometry (QLSI) [42-45]. A LED with a wavelength centered at 617 nm integrated in a Köhler configuration is used as an illumination source with a controlled optical plane wave (controlled illuminated area and controlled numerical aperture). The light beam passing through the metasurface is collected by a microscope objective and sent to the QLSI wavefront analyzer (SID4 camera from Phasics Company) to measure both the intensity and the optical path difference of the light at the microscope's imaging plane, coinciding with the metasurface position.

References

- [1] Anderson R, Moore T. The Economics of Information Security. *Science* 2006; 314: 610–3.
- [2] Whitman ME, Mattord HJ. Principles of information security. Cengage Learning, 2011.
- [3] Matoba O, Nomura T, Perez-Cabre E, Millan MS, Javidi B. Optical Techniques for Information Security. *Proceedings of the IEEE* 2009; 97: 1128–48.
- [4] Javidi B, editor. Optical and digital techniques for information security. New York: Springer, 2005.

- [5] Lippmann G. Sur la théorie de la photographie des couleurs simples et composées par la méthode interférentielle. *J Phys Theor Appl* 1894; 3: 97–107.
- [6] Li Y, Kreske K, Rosen J. Security and encryption optical systems based on a correlator with significant output images. *Appl Opt*, AO 2000; 39: 5295–301.
- [7] Bryngdahl O, Wyrowski F. I Digital Holography – Computer-Generated Holograms. In: Wolf E, editor. *Progress in Optics*. Elsevier, 1990; 28: 1–86.
- [8] Yu N, Genevet P, Kats MA, et al. Light Propagation with Phase Discontinuities: Generalized Laws of Reflection and Refraction. *Science* 2011; 334: 333–7.
- [9] Yu N, Capasso F. Flat optics with designer metasurfaces. *Nat Mater* 2014; 13: 139–50.
- [10] Genevet P, Capasso F, Aieta F, Khorasaninejad M, Devlin R. Recent advances in planar optics: from plasmonic to dielectric metasurfaces. *Optica* 2017; 4: 139–52.
- [11] Khorasaninejad M, Capasso F. Metalenses: Versatile multifunctional photonic components. *Science* 2017; 358: eaam8100.
- [12] Chen WT, Zhu AY, Sanjeev V, et al. A broadband achromatic metalens for focusing and imaging in the visible. *Nat Nanotechnol* 2018; 13: 220–6.
- [13] Wang S, Wu PC, Su V-C, et al. A broadband achromatic metalens in the visible. *Nat Nanotechnol* 2018; 13: 227–32.
- [14] Sun C. Shrinking the camera size: Metasurface lens. *Nat Mater* 2017; 16: 11–2.
- [15] Zhu WM, Song Q, Yan L, et al. A flat lens with tunable phase gradient by using random access reconfigurable metamaterial. *Adv Mater* 2015; 27: 4739–43.
- [16] Teo JYH, Wong LJ, Molardi C, Genevet P. Controlling electromagnetic fields at boundaries of arbitrary geometries. *Phys Rev A* 2016; 94: 023820.
- [17] Xie YY, Ni PN, Wang QH, et al. Metasurface-integrated vertical cavity surface-emitting lasers for programmable directional lasing emissions. *Nat Nanotechnol* 2020; 15: 125–30.
- [18] Zheng G, Mühlenbernd H, Kenney M, Li G, Zentgraf T, Zhang S. Metasurface holograms reaching 80% efficiency. *Nat Nanotechnol* 2015; 10: 308–12.
- [19] Genevet P, Lin J, Kats MA, Capasso F. Holographic detection of the orbital angular momentum of light with plasmonic photodiodes. *Nat Commun* 2012; 3: 1278.
- [20] Huang L, Chen X, Mühlenbernd H, et al. Three-dimensional optical holography using a plasmonic metasurface. *Nat Commun* 2013; 4: 2808.
- [21] Song Q, Baroni A, Sawavt R, et al. Ptychography retrieval of fully polarized holograms from geometric-phase metasurfaces. *Nat Commun* 2020; 11: 1–8.
- [22] Gansel JK, Thiel M, Rill MS, et al. Gold Helix Photonic Metamaterial as Broadband Circular Polarizer. *Science* 2009; 325: 1513–5.
- [23] Song QH, Wu PC, Zhu WM, et al. Split Archimedean spiral metasurface for controllable GHz asymmetric transmission. *Appl Phys Lett* 2019; 114: 151105.
- [24] Shi YZ, Zhu T, Zhang T, et al. Chirality-assisted lateral momentum transfer for bidirectional enantioselective separation. *Light Sci Appl* 2020; 9: 1–12.
- [25] Akselrod GM, Huang J, Hoang TB, et al. Large-Area Metasurface Perfect Absorbers from Visible to Near-Infrared. *Adv Mater* 2015; 27: 8028–34.
- [26] Song Q, Zhu WM, Wu PC, et al. Liquid-metal-based metasurface for terahertz absorption material: frequency-agile and wide-angle. *APL Mater* 2017; 5: 066103.
- [27] Yan L, Zhu WM, Karim MF, et al. 0.2 λ_0 thick adaptive retroreflector made of spin-locked metasurface. *Adv Mater* 2018; 30:1802721.
- [28] Kumar K, Duan H, Hegde RS, Koh SC, Wei JN, Yang JK. Printing colour at the optical diffraction limit. *Nat Nanotechnol* 2012; 7:557–61.
- [29] Gu Y, Zhang L, Yang JK, Yeo SP, Qiu CW. Color generation via subwavelength plasmonic nanostructures. *Nanoscale* 2015; 7: 6409–19.
- [30] Luo X, Hu Y, Li X, et al. Integrated Metasurfaces with Microprints and Helicity- Multiplexed Holograms for Real- Time Optical Encryption. *Adv Opt Mater* 2020; 8: 1902020.
- [31] Zhao R, Huang L, Tang C, et al. Nanoscale Polarization Manipulation and Encryption Based on Dielectric Metasurfaces. *Adv Opt Mater* 2018; 6: 1800490.
- [32] Deng J, Deng L, Guan Z, et al. Multiplexed Anticounterfeiting Meta-image Displays with Single-Sized Nanostructures. *Nano Lett* 2020; 20: 1830–8.
- [33] Deng L, Deng J, Guan Z, et al. Malus-metasurface-assisted polarization multiplexing. *Light Sci Appl* 2020; 9:101.
- [34] Ren H, Briere G, Fang X, et al. Metasurface orbital angular momentum holography. *Nat Commun* 2019; 10:2986.
- [35] Fang X, Ren H, Gu M. Orbital angular momentum holography for high-security encryption. *Nat Photonics* 2020; 14: 102–8.
- [36] Chen K, Ding G, Hu G, et al. Directional Janus Metasurface. *Adv Mater* 2020; 32: 1906352.
- [37] Chen Y, Yang X, Gao J. 3D Janus plasmonic helical nanoapertures for polarization-encrypted data storage. *Light Sci Appl* 2019; 8:45.
- [38] Frese D, Wei Q, Wang Y, Huang L, Zentgraf T. Nonreciprocal Asymmetric Polarization Encryption by Layered Plasmonic Metasurfaces. *Nano Lett* 2019; 19: 3976–80.
- [39] Yoon G, Lee D, Nam KT, Rho J. “Crypto-Display” in Dual-Mode Metasurfaces by Simultaneous Control of Phase and Spectral Responses. *ACS Nano* 2018; 12: 6421–8.
- [40] Lim KTP, Liu H, Liu Y, Yang JKW. Holographic colour prints for enhanced optical security by combined phase and amplitude control. *Nat Commun* 2019; 10:25.

- [41] Deng J, Yang Y, Tao J, et al. Spatial Frequency Multiplexed Meta-Holography and Meta-Nanoprinting. *ACS Nano* 2019; 13: 9237-46.
- [42] Li J, Kamin S, Zheng G, Neubrech F, Zhang S, Liu N. Addressable metasurfaces for dynamic holography and optical information encryption. *Sci Adv* 2018; 4: eaar6768.
- [43] Bon P, Maucort G, Wattellier B, Monneret S. Quadriwave lateral shearing interferometry for quantitative phase microscopy of living cells. *Opt Express* 2009; 17: 13080.
- [44] Khadir S, Andr n D, Chaumet PC, et al. Full optical characterization of single nanoparticles using quantitative phase imaging. *Optica* 2020; 7: 243.
- [45] Khadir S, Andr n D, Verre D, et al. Metasurface characterization using quadriwave lateral shearing interferometry. Submitted 2020.
- [46] Primot J, Gu rineau N. Extended Hartmann test based on the pseudoguiding property of a Hartmann mask completed by a phase chessboard. *Appl Opt* 2000 ; 39 :5715-20.
- [47] Colburn S, Zhan A, Bayati E, et al. Broadband transparent and CMOS-compatible flat optics with silicon nitride metasurfaces. *Opt Mater Express* 2018 ; 8 :2330-43.
- [48] Khorasaninejad M, Chen WT, Devlin RC, Oh J, Zhu AY, Capasso F. Metalenses at visible wavelengths : Diffraction-limited focusing and subwavelength resolution imaging. *Science* 2016 ; 352 :1190-94.